



Cite this: DOI: 10.1039/c7ta01398a

# Rh-promoted mixed oxides for “low-temperature” methane partial oxidation in the absence of gaseous oxidants†

Arya Shafiefarhood,‡ Junshe Zhang,‡ Luke Michael Neal and Fanxing Li \*

Compared to conventional reforming, chemical looping reforming (CLR), which partially oxidizes methane in the absence of gaseous oxidants such as steam or oxygen, offers a simpler and potentially more efficient route for syngas generation. This is achieved by cyclic removal and replenishment of active lattice oxygen in oxygen carrier particles, a.k.a. redox catalysts. With redox catalysts being at the heart of CLR, their activity and selectivity are crucial for the CLR performance. While many redox catalysts have been developed, their activities toward methane partial oxidation (POx), especially at relatively low temperatures, are often limited due to the high activation energy for the migration and removal of lattice oxygen. Moreover, syngas selectivity is often less than ideal due to the non-selective nature of the surfaces for many oxides. To address these limitations, we investigated the effects of promoting the catalytic activity of oxide surfaces for two redox catalysts:  $\text{CaMnO}_3$  and  $\text{LaCeO}_3$ . Our findings indicate that promoting mixed oxides with a small amount of Rh can lower the onset temperature of methane POx by as much as 300 °C (0.5 wt% Rh loading). Over 93% syngas selectivity and 7.9 mmol of syngas per gram of redox catalyst were obtained for a highly stable, Rh promoted  $\text{CaMnO}_3$  at 600 °C, making it a promising redox catalyst for methane POx under a cyclic redox scheme.

Received 15th February 2017  
Accepted 11th April 2017

DOI: 10.1039/c7ta01398a

rsc.li/materials-a

## Introduction

Methane, the primary component of natural gas, is the most abundant organic compound on earth.<sup>1</sup> Its relative abundance and lower  $\text{CO}_2$  emission compared to petroleum and coal have led to renewed interest in the conversion of methane to value-added products such as liquid transportation fuels and chemicals. Although the direct conversion of methane to chemicals such as oxygenates, olefins, and aromatics has been extensively investigated within the scientific community, it has yet to demonstrate feasible product yields from an economic viewpoint.<sup>2</sup> To date, commercial methane valorization processes are exclusively based on indirect approaches: methane is first reformed into syngas, *i.e.* a mixture of CO and  $\text{H}_2$ ; subsequently, the syngas stream is conditioned and converted into desired products.<sup>3–6</sup> As a crucial first step, methane reforming is both capital intensive and inefficient due to coke formation, catalyst deactivation, high endothermicity, significant steam requirements, and/or the needs for cryogenic air separation units (ASU).

Compared to conventional methane reforming, chemical looping reforming (CLR) offers a potentially more efficient route that eliminates the need for ASU.<sup>7,8</sup> This is realized through redox active oxygen carriers, a.k.a. redox catalysts, which incorporate oxygen from air into their lattice. The active lattice oxygen is subsequently donated for methane partial oxidation (POx). Two interconnected reactors are used to complete such a cyclic redox process. Due to their critical importance for CLR, numerous research efforts have been devoted to selection and synthesis of more active and selective redox catalysts.<sup>7–13</sup> A typical redox catalyst is composed of an oxygen reservoir, which is commonly a first row transition metal oxide, and an inert support to increase its stability and oxygen mobility.<sup>7,8</sup> Although proven to be effective, the aforementioned oxides face such challenges as high cost, low activity, and/or limited selectivity. Nickel based oxides are one of the more extensively studied materials. Their application, however, is hindered due to high cost, health and environmental concerns, and coking and sulfur poisoning issues.<sup>14–19</sup> The use of iron and manganese based oxides can be advantageous as they are abundant and environmentally benign, but they exhibited low syngas selectivity.<sup>7,8</sup> Our recent studies showed that mixed metal oxides, such as perovskites, can be used as supports to both increase the mechanical integrity of the oxygen reservoir and provide metallic catalytic sites for methane partial oxidation.<sup>20–28</sup> It is noted that such catalytic sites are only present in (partially) reduced redox catalysts.<sup>22,24</sup> Moreover, partially exposed iron

North Carolina State University, Chemical and Biomolecular Engineering, USA.  
E-mail: fli5@ncsu.edu

† Electronic supplementary information (ESI) available. See DOI: 10.1039/c7ta01398a

‡ First authors.

oxide phases negatively impact the methane to syngas selectivity.

To improve the selectivity of redox catalysts, two potential strategies can be adopted. The first approach is thermodynamically inhibiting over-oxidation by designing redox catalysts with suitable equilibrium oxygen partial pressures ( $P_{O_2}$ ). Several recent studies reported improved syngas selectivity using oxygen carriers and reactor configurations that are thermodynamically selective.<sup>27,29</sup> The second approach is to prepare redox catalysts with more selective surfaces. One example is core-shell structured redox catalysts with a nonselective oxygen reservoir as the core and a selective perovskite phase as the shell.<sup>21,26</sup> The selectivity of such redox catalysts, however, is limited by their surface oxidation state, which is determined by relative rates of bulk lattice oxygen diffusion and surface oxygen removal. The surface (or loosely bound) oxygen species of oxidized redox catalysts were found to be responsible for the non-selective combustion reactions.<sup>22</sup> This leads to a non-selective region at the beginning of the methane oxidation reaction.<sup>22,24,27</sup> Although partially reoxidizing the core-shell redox catalyst can significantly enhance the syngas selectivity,<sup>24</sup> it reduces the overall oxygen carrying capacity and increases the complexity of the process. It is also noted that most redox catalysts reported to date require high operating temperatures (>800 °C); this is primarily due to the low surface activity for methane activation and the high activation energy required for lattice oxygen and/or cation migration.<sup>7,8</sup>

The current work investigates an alternative strategy to improve the surface catalytic activity of mixed metal oxides and to enhance the redox activity of these oxides at significantly lower temperatures. Rh is selected as the promoter since it is readily reducible and highly effective for methane activation.<sup>30-35</sup> Although Rh is active for methane combustion under oxidizing environments, the  $O_2$  free environment in CLR allows for high methane conversion activity and syngas selectivity.<sup>36-38</sup> In terms of oxygen carrying materials, two mixed-oxides with different equilibrium  $P_{O_2}$ , *i.e.*  $CaMnO_3$  and  $LaCeO_{3.5}$ , are selected.  $CaMnO_3$  has “oxygen uncoupling” properties and spontaneously releases oxygen at elevated temperatures due to its high equilibrium  $P_{O_2}$ .  $LaCeO_{3.5}$ , on the other hand, has low equilibrium  $P_{O_2}$  which is desirable for POx reactions from a syngas selectivity standpoint. Since these mixed oxides possess both redox activity and mixed conductive properties, they are highly recyclable without an inert support.

Our results indicate that the relative rates of lattice oxygen ( $O^{2-}$ ) conduction to the surface and the surface oxygen removal by the gas-solid reactions determine the selectivity of the redox catalysts. This is particularly the case at the early stage of the reaction. The presence of Rh on the surface increases the oxygen removal rate from the surface and hence inhibits the formation of nonselective surface oxygen species. This is realized by the enhancement of methane activation and hence more effective oxygen removal from the surface. It is also noted that the rate of bulk lattice oxygen diffusion controls the overall reaction rate for later stages of the reaction. Such a diffusion rate can be notably affected by the surface of the redox catalysts, which provides the driving force for  $O^{2-}$  conduction. As such,

the Rh-promoter significantly increases the activity of the catalysts at lower temperatures. For instance, the Rh-promoter reduces the onset temperature of the POx reaction by up to 300 °C. While un-promoted  $CaMnO_3$  exhibits very low activity/selectivity below 800 °C, the promoted sample exhibited a maximum CO yield at 600 °C with CO selectivity above 86% and remained active at 500 °C. Although  $LaCeO_{3.5}$  exhibits high syngas selectivity at high temperatures (900 °C), it suffers from slow kinetics and becomes significantly less active below 800 °C. Promoting the  $LaCeO_{3.5}$  with Rh not only improves the kinetics at high temperatures, but also reduces the onset temperature for methane conversion to 600 °C.

## Experimental

### Redox catalyst synthesis

Two redox catalysts were synthesized for this study:  $CaMnO_3$  and  $LaCeO_{3.5}$ . The samples were prepared using a modified Pechini method. Details of the method are described elsewhere.<sup>21</sup> In short, stoichiometric amounts of nitrate salts of lanthanum and cerium, or calcium and manganese were dissolved in deionized water and stirred for 30 minutes at room temperature to form a homogeneous solution. Citric acid is added to the solution with a molar ratio of 2.5 : 1 of citric acid and total cations, and the solution is kept under stirring for another half an hour at 60 °C. Ethylene glycol with a molar ratio of 1.5 : 1 with respect to citric acid was then added to the solution, and the temperature of the solution is increased to 80 °C under stirring until a homogeneous gel is formed. The gel is then dried overnight at 100 °C and annealed at 950 °C for 8 hours.

The surface of the synthesized redox catalysts was also promoted with rhodium using an incipient wetness method (0.5 wt% Rh). Rhodium nitrate salt was dissolved in deionized water and appropriate amounts of the solution were added to the samples in multiple steps. The impregnated samples were then dried at 100 °C for 4 hours and fired at 950 °C for 6 hours. We note that although the cost of Rh can be prohibitive for conventional, circulating fluid bed based CLR; the current study focuses on mechanistic investigations of the effects of surface promotion. Moreover, the high activity exhibited by the Rh-promoted redox catalysts at low temperatures offers the opportunities to use such redox catalysts in simplified fixed bed systems to minimize attrition and particle loss.

### Sample characterization

Powder X-ray diffraction (XRD) experiments were performed. XRD patterns were obtained using a Rigaku SmartLab X-ray diffractometer with  $Cu-K\alpha$  ( $\lambda = 0.1542$ ) radiation operating at 40 kV and 44 mA. A stepwise approach with a step size of  $0.1^\circ$  and residence time of 2.5 seconds at each step in the  $20-80^\circ$  angle range ( $2\theta$ ) was used to generate the XRD patterns. Similar experiments were also performed on the spent samples to confirm their phase stability. X-ray photoelectron spectroscopy (XPS, Thermo Fisher Scientific Inc.) with an  $Al-K\alpha$  X-ray source at an operating voltage of 20 kV and a current of 10 mA is used to analyze near surface elemental compositions. Survey spectra

and the single element spectra were collected with 20 eV and 100 eV pass energy. The BET surface areas of the samples are determined using a Micromeritics ASAP 2020 physico-adsorption system with krypton as the adsorption gas. Diffuse reflectance infrared Fourier transform spectroscopy (DRIFTS) is also performed on the selected samples to distinguish their different surface activation and intermediate species. DRIFTS measurements are performed in an *in situ* reaction cell (Pike Technologies DiffuseIR cell) that allowed continuous gas flow through the samples. The spectra are collected on a Thermo Scientific Nicolet iS50 FT-IR spectrometer equipped with a MCT/A detector and a KBr beam splitter and optics using 128 scans at 4 cm<sup>-1</sup> resolution. The CO desorption experiments were performed on the reduced samples (50% H<sub>2</sub> balance Ar, 700 °C, 1 hour). The samples were exposed to CO (grade 5.0, 50% balance Ar) at room temperatures and spectra were collected after purging the system with argon.

### Redox experiments

The reducibility of the samples in methane was tested through temperature programmed reduction (TPR) experiments. The experiments were performed in a thermal gravimetric analyzer (TGA, Q600 TA Instruments) and in 10 vol% methane (grade 5.0, balance Ar). The temperature was increased from room temperature to 1000 °C with a 20 °C min<sup>-1</sup> ramping rate and kept isothermal for 30 minutes. The samples were oxidized at 900 °C in 20% oxygen (ultra-dry, balance Ar) for 30 minutes prior to the experiments.

Redox experiments were performed in a fixed bed configuration and in a quartz U-tube reactor (1/8" ID) with 50 mg sample loading, 100 ml min<sup>-1</sup> total flow rate, and 10 vol% reactive gases (CH<sub>4</sub> and O<sub>2</sub>) approximating a differential bed reactor. The reactor was purged with argon after each half cycle to prevent mixing of the reactive gases. The samples were held in place using quartz wool to prevent fluidization of the particles. The reactor effluent was analyzed using a quadrupole mass spectrometer (Cirrus 2, MKS). To ensure the accuracy of the qualitative analysis, a single point calibration was performed using a standard calibration gas (1% H<sub>2</sub>, 1% CH<sub>4</sub>, 1% CO, and 1% CO<sub>2</sub>, balance Ar) before each experiment.

The same reactor configuration was used to perform the pulse injection and co-feed (CH<sub>4</sub> and O<sub>2</sub>) experiments. The detailed gas delivery configuration was presented elsewhere.<sup>22</sup> Co-feed experiments were done with 5 different methane to oxygen ratios (CH<sub>4</sub>/O<sub>2</sub> = 1.5, 1, 0.5, 0.2, and 0.1) to investigate the selectivity and methane conversion of the samples at different surface oxidation states. The concentrations of methane were kept below the flammability limit in all experiments. The pulse injection configuration is demonstrated in Fig. S1† and explained in detail elsewhere.<sup>22</sup> This configuration allows injection of small amounts of reactive gases on the catalyst to observe the behavior of the catalyst with minimal change in its bulk properties. This also allows conducting methane isotope exchange experiments by co-injection of methane and deuterated methane and monitoring the exchange products.

## Results and discussion

### Redox catalyst selection and characterization

Two redox catalysts are chosen for the current study: CaMnO<sub>3</sub> and LaCeO<sub>3.5</sub>. Calcium manganate is one of the most studied mixed oxides for chemical looping applications.<sup>7,8,39</sup> Most of the previous studies, however, focused on its CLOU properties as it exhibits poor syngas selectivity, as one would anticipate from its high equilibrium P<sub>O<sub>2</sub></sub> and catalytic activity for methane combustion. The low selectivity of un-promoted CaMnO<sub>3</sub> makes it an excellent candidate to investigate the effects of the Rh promoter.

Ceria (CeO<sub>2</sub>) is another well-known material as both an oxygen carrier and support in chemical looping applications.<sup>40-43</sup> Ceria is a particularly interesting material as it is redox active and has excellent syngas selectivity and mixed conductivity.<sup>44,45</sup> However, it suffers from poor reduction kinetics. A recent study also showed that it can trigger deactivation when used as a support for iron oxide.<sup>25</sup> Addition of lanthanum to ceria can potentially enhance the reduction kinetics of ceria. It can also hinder coke formation by increasing the surface basicity. In this study, LaCeO<sub>3.5</sub> is chosen as addition of more than 50% lanthanum to CeO<sub>2</sub> is reported to cause phase segregation whereas LaCeO<sub>3.5</sub> forms a stable structure with desirable P<sub>O<sub>2</sub></sub> for methane partial oxidation.<sup>46</sup> Our preliminary results confirm excellent methane partial oxidation selectivity and coke resistance on LaCeO<sub>3.5</sub>. However, it shows very slow kinetics. This makes it ideal for probing the kinetic improvements with the Rh promoter. Both redox catalysts are prepared through a modified Pechini method. XRD results (Fig. S2†) confirmed the formation of cubic fluorite and orthorhombic perovskite structures for LaCeO<sub>3.5</sub> and CaMnO<sub>3</sub> samples respectively. The surface of the catalysts is then impregnated with 0.5 wt% rhodium (metallic basis) using a wet impregnation method. The XRD patterns of the Rh-promoted samples are nearly identical to those of unpromoted samples (Fig. S2†). Rietveld refinement analysis indicates very minor changes in the lattice parameters of the samples (Table S1†). Similar experiments were also performed on the spent samples to confirm their phase stability. Fig. S3† shows the XRD pattern of the Rh-promoted CaMnO<sub>3</sub> after 5 redox cycles at 900 °C and 10% CH<sub>4</sub>/O<sub>2</sub>. No major structural change was observed on the sample after redox cycles.

### Methane TPR experiments

TPR experiments were performed to investigate the effect of Rh on the reactivity of the redox catalysts in methane. Differential thermal gravimetric (DTG) analysis was used to determine the reduction temperatures of the samples in methane. Fig. 1 compares the DTG data of the promoted and un-promoted redox catalysts (weight loss data in Fig. S4†). It is obvious that the presence of Rh changes their reduction properties. The initial reduction temperature of CaMnO<sub>3</sub> decreased by almost 200 °C when Rh is present. Similarly, the Rh promoted LaCeO<sub>3.5</sub> started to reduce at around 600 °C whereas the unpromoted sample did not show any significant reduction until 950 °C. The

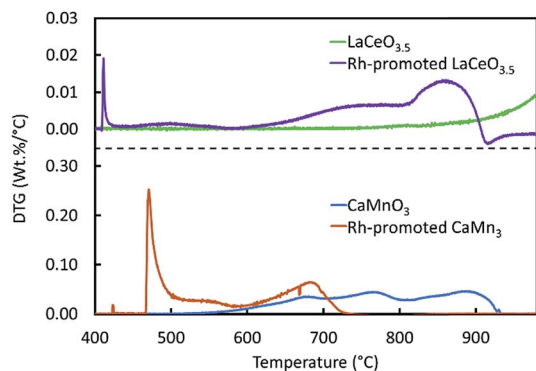


Fig. 1 DTG results of redox catalysts in methane TPR experiments ( $20\text{ }^{\circ}\text{C min}^{-1}$  ramping rate).

larger weight loss at lower temperatures can be attributed to changes in the surface and/or bulk properties of the redox catalyst. Rh is known to promote methane activation.<sup>30,33</sup> Therefore, the presence of Rh on the surface of the redox catalyst can significantly enhance methane activation, leading to more effective oxygen removal at lower temperatures. In addition to surface enhancement, Rh could also be incorporated into the perovskite bulk structure;<sup>47</sup> this can alter the thermodynamic and/or ionic conduction properties of the redox catalyst. The peaks observed at lower temperatures ( $\sim 420\text{ }^{\circ}\text{C}$ ) are attributed to rhodium oxide reduction as they appear only in the case of the promoted samples. It is also evident that the oxygen carrying capacities of  $\text{CaMnO}_3$  based redox catalysts are

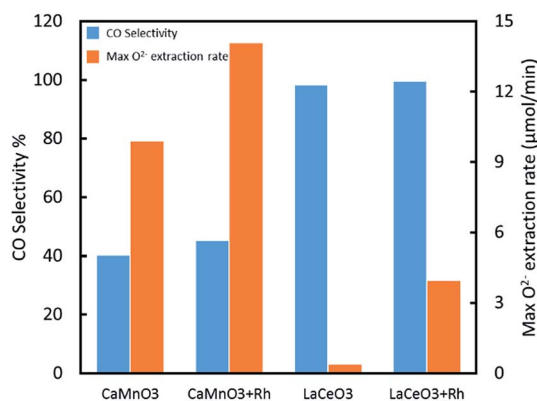


Fig. 2 Comparison of the CO selectivity and maximum oxygen donation rate of the redox catalysts at  $900\text{ }^{\circ}\text{C}$ .

significantly higher than those of their  $\text{LaCeO}_{3.5}$  counterparts (Fig. S4†).

### Methane–oxygen redox testing

The activity, selectivity, and coke resistance of the redox catalysts were tested in a U-tube reactor. Redox experiments were performed by alternating the reactor feed at  $900\text{ }^{\circ}\text{C}$ . A relatively low gas residence time was used to ensure low ( $\leq 15\%$ ) methane/oxygen conversion, in order to approximate a differential bed operation. Coke formation was quantified by calculating the amount of CO and  $\text{CO}_2$  produced during the oxidation half cycle. Fig. 2 compares the CO selectivity and oxygen donation rate of the samples during the reduction half cycle in the 5<sup>th</sup> redox cycle (the product concentration profiles are shown in Fig. S5†). The CO and  $\text{H}_2$  selectivity,  $\text{CH}_4$  conversion, and coke formation data for the same cycle are summarized in Table 1.

As anticipated, the two unpromoted mixed oxides behave substantially different. Calcium manganate shows a faster but less selective conversion of methane (Fig. S5a†) while lanthanum ceria is more selective but with a much lower conversion rate (Fig. S5c†). Both samples showed a non-selective region at the beginning of the POx reaction. This non-selective region is considerably more prominent for the  $\text{CaMnO}_3$  sample and is typically attributed to surface and/or loosely bound oxygen species. After the initial  $\text{CO}_2$  peaks, both samples become selective towards methane POx.

The presence of Rh significantly affects both selectivity and methane conversion. Lanthanum ceria undergoes a substantial kinetic improvement when promoted with Rh (Fig. S5d†). The presence of Rh increases the maximum oxygen donation rate by more than 11 times. A slight increase in CO selectivity is also observed. The kinetic improvement is less significant for calcium manganate, which is already highly active at  $900\text{ }^{\circ}\text{C}$  without promoters. Nevertheless, 40% improvement in the rate of oxygen removal was observed (Fig. 3). A slight increase is observed in both CO and  $\text{H}_2$  selectivities. This is attributed to the presence of metallic rhodium on the surface as will be discussed later.

Addition of Rh increases the amounts of methane conversion and oxygen donation by about 20 and 8% respectively for these oxides. This increase in oxygen donation cannot be from the rhodium oxide reduction as reduction of  $\text{Rh}_2\text{O}_3$  to Rh would have accounted for no more than 0.02 wt% oxygen, which is significantly lower than the observed oxygen capacity increase. One potential explanation is that Rh is incorporated into the bulk structures of the mixed oxides, thereby changing their

Table 1 Methane conversion,  $\text{CO}/\text{H}_2$  selectivity, oxygen donation, and coke formation of the redox catalysts during the reduction half cycle at  $900\text{ }^{\circ}\text{C}$

Sample	CO selectivity%	$\text{H}_2$ selectivity% (excluding $\text{H}_2$ from coke)	$\text{H}_2$ selectivity% (including $\text{H}_2$ from coke)	$\text{CH}_4$ converted (ml)	$\text{O}_2$ extracted (wt%)	Coke formation (wt%)
$\text{CaMnO}_3$	40.08	29.34	37.18	2.13	9.18	0.29
$\text{CaMnO}_3 + \text{Rh}$	44.93	40.30	46.47	2.59	10.17	0.32
$\text{LaCeO}_{3.5}$	98.21	86.76	87.69	2.13	3.91	0.17
$\text{LaCeO}_{3.5} + \text{Rh}$	99.46	90.11	91.26	2.54	4.36	0.36

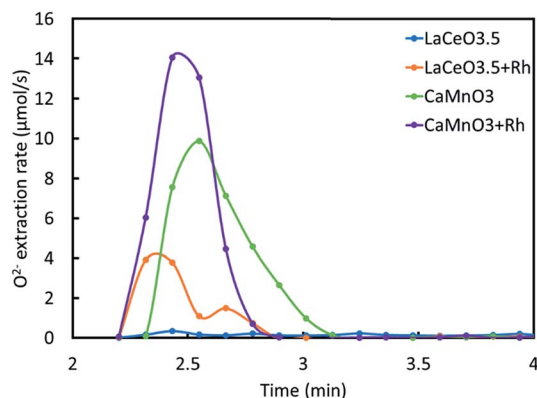


Fig. 3 Oxygen extracted from the redox catalysts during the initial stages of the reduction at 900 °C in 10% methane.

thermodynamic properties. This is not likely due to the very similar crystal structures of the samples (Table S1†). The other possible explanation is the kinetic effect as the presence of Rh on the surface can improve methane activation. Enhancements in surface reaction rates can in turn accelerate the rates of lattice oxygen removal and increase oxygen carrying capacity of the redox catalysts under the 15 min reduction half cycle.

To shed light on the role of Rh, XPS experiments were performed. Table 2 summarizes the near surface concentrations of the elements in both oxidized and reduced forms after five complete redox cycles at 900 °C. The near surface concentration of Rh on LaCeO<sub>3.5</sub> and CaMnO<sub>3</sub> remained 3–5 times higher than the nominal amount of Rh added. This confirms that rhodium is enriched on the surface. Hence, improving the surface methane activation is likely to be the primary reason for the enhanced redox performance. Due to the low surface areas of the samples (0.29 and 0.39 m<sup>2</sup> g<sup>-1</sup> for the as-prepared and cycled Rh-promoted CaMnO<sub>3</sub>), it is difficult to obtain reliable data on Rh dispersion on the redox catalysts using chemisorption-based approaches.

### Methane conversion in the presence of gaseous oxygen

To determine the effect of Rh on surface methane activation, methane–oxygen co-feed experiments are conducted. Five

oxygen to methane ratios were used (O<sub>2</sub>/CH<sub>4</sub>: 1.5, 1, 0.5, 0.2, and 0.1). The results of LaCeO<sub>3.5</sub>-based samples are shown in Fig. 4. As expected, the CO selectivity on the un-promoted LaCeO<sub>3</sub> increased from 9.5% to 44.7% with decreasing O<sub>2</sub> : CH<sub>4</sub> ratio. In comparison, CO selectivity is 98.2% in the O<sub>2</sub>-free redox mode. This indicates that surface/loosely bound oxygen species are likely to be responsible for methane combustion. In addition, the redox reaction is likely to be limited by bulk lattice oxygen conduction as evidenced by significantly higher methane conversion in the presence of gaseous oxygen. The immediate shift in selectivity observed on the un-promoted samples in the redox mode indicates that the formation of non-selective surface oxygen species is inhibited in the absence of gaseous oxygen. Similar trends are observed with the CaMnO<sub>3</sub>-based samples (Fig. S6†).

Rh-promoted catalysts show notably different results. Methane conversion increases with oxygen concentrations and plateaus around 70% at O<sub>2</sub> : CH<sub>4</sub> ratios above 1 : 1. Higher methane conversion is observed at low O<sub>2</sub> : CH<sub>4</sub> ratios compared to the un-promoted sample. This indicates that the presence of reduced Rh on the surface catalyzes methane activation. The promoted sample also showed improved CO selectivity, especially at lower O<sub>2</sub> : CH<sub>4</sub> ratios (Fig. S7a and S8a†). These observations illustrate that the presence of Rh on the surface substantially changes the methane activation rate and mechanism. This is also corroborated by the methane isotope exchange studies below.

### Methane isotope exchange

Isotope exchange experiments were performed to investigate methane activation on the promoted and un-promoted samples. An equimolar mixture of CH<sub>4</sub> and CD<sub>4</sub> (25% each, balance Ar) was injected to the redox catalysts at elevated temperatures. The ratios of CHD<sub>3</sub> (*m/z* = 19) and CD<sub>4</sub> (*m/z* = 20) signals are used to quantify the degree of methane activation on redox catalysts. These two mass/charge signals are chosen as they do not have partial contributions from the other exchange products. Fig. 5 summarizes the results of the first 10 pulse injections at 800 °C. It is evident that the un-promoted and Rh-

Table 2 Near surface atomic elemental composition of the redox catalysts in the reduced and oxidized state after 5 methane/oxygen cycles based on XPS analysis

Element	Average based on Rh-loading	Un-promoted-Ox	Rh-promoted Ox	Un-promoted Red	Rh-promoted Red
<b>LaCeO<sub>3.5</sub></b>					
Ce	18.13	5.27	5.62	3.49	4.26
La	18.13	12.65	11.58	14.16	12.26
Rh	0.30	0.00	1.52	0.00	1.18
O	63.45	82.08	81.28	82.35	82.31
<b>CaMnO<sub>3</sub></b>					
Mn	19.97	8.97	8.66	5.73	5.98
Ca	19.97	23.52	23.88	24.23	23.07
Rh	0.14	0.00	0.43	0.00	0.67
O	59.92	67.51	67.03	70.03	70.27

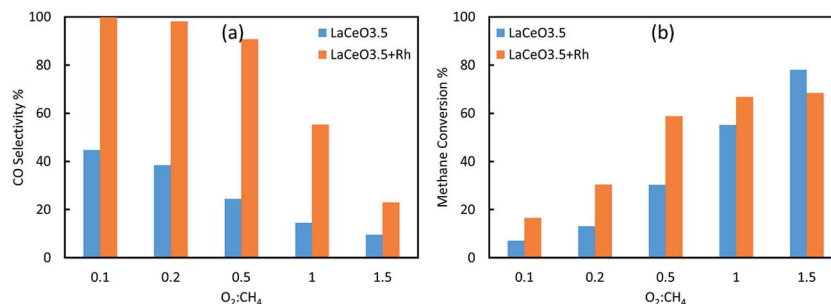


Fig. 4 Comparison of (a) CO selectivity and (b) methane conversion during methane–oxygen co-feed experiments using un-promoted and Rh-promoted LaCeO<sub>3.5</sub>-based redox catalysts at 900 °C.

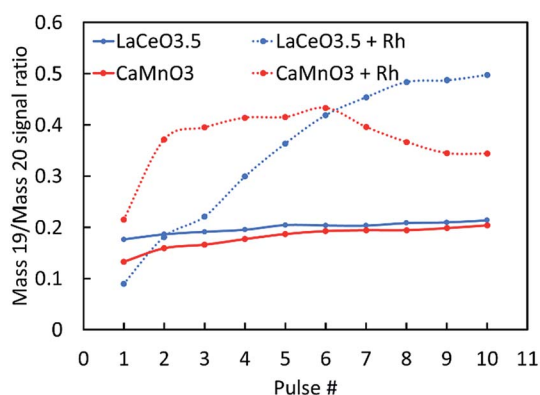


Fig. 5 Comparison of methane isotope exchange on the redox catalysts at 800 °C.

promoted samples behave significantly different. While the methane exchange remains relatively constant on the un-promoted samples during 10 pulse injections, it increased by up to 400% on the Rh-promoted samples, especially during the first 5 pulses. This indicates that reduced Rh significantly enhances methane activation and surface coverage of intermediate species from methane dissociation. The presence of metallic Rh on the surface is further confirmed by DRIFTS with CO temperature programmed desorption. The un-promoted and Rh-promoted LaCeO<sub>3.5</sub> samples showed markedly different IR-spectra for adsorbed CO species (Fig. S9†). The unpromoted sample only shows the formation of carbonate species (1300–1600 cm<sup>-1</sup>) at room temperature. The Rh-promoted sample, in

comparison, also forms carbonyl species (1980–2110 cm<sup>-1</sup>). These carbonyl groups are stable until above 200 °C and give rise to gaseous CO<sub>2</sub> species (2300–2400 cm<sup>-1</sup>) at higher temperatures.

### Transient pulse experiments

Pulse experiments were performed to investigate the effect of bulk oxygen conduction and surface evolution on the conversion and selectivity of the catalysts. Two different relaxation times of 30 seconds and 2 minutes were used between the 20 methane (50 vol% balance Ar) pulses injected. The relaxation allows identification of potential O<sup>2-</sup> conduction limitations.<sup>22</sup> Fig. 6 and 7 show the CO selectivity and oxygen removal at 900 °C during each pulse for CaMnO<sub>3</sub>-based and LaCeO<sub>3.5</sub>-based redox catalysts respectively. The un-promoted CaMnO<sub>3</sub> sample demonstrates non-selective behavior regardless of the relaxation time. This indicates a faster O<sup>2-</sup> supply from the bulk when compared to the rate of oxygen removal from the surface. The Rh-promoted sample, however, shows a transition to selective partial oxidation after the first few pulses. This transition is consistent with the generation of reduced Rh on the surface.

Pulse injection on the LaCeO<sub>3.5</sub>-based redox catalysts clearly shows that a higher relaxation time leads to a less selective behavior on the un-promoted sample. Significantly less oxygen extraction and methane conversion were also observed during the pulse injection on the un-promoted catalyst (Fig. 7). This is consistent with the poor methane activation and slow overall kinetics of the LaCeO<sub>3</sub> redox catalyst combined with low methane concentration in the pulse injection configuration.

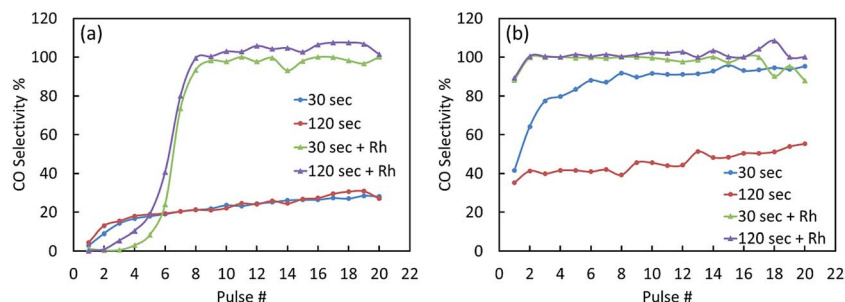


Fig. 6 Comparison of CO selectivity at each methane pulse injection on (a) CaMnO<sub>3</sub>-based and (b) LaCeO<sub>3.5</sub>-based redox catalysts at 900 °C.

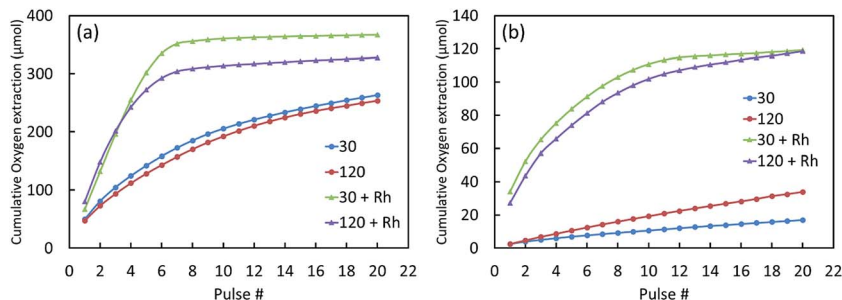


Fig. 7 Comparison of cumulative oxygen donation during 20 methane pulse injections on (a)  $\text{CaMnO}_3$ -based and (b)  $\text{LaCeO}_{3.5}$ -based redox catalysts at  $900^\circ\text{C}$ .

Further analysis of the pulses shows that at a similar oxygen content (after the 5<sup>th</sup> pulse with 2 min relaxation and 10<sup>th</sup> pulse with 30 s relaxation), >250% more oxygen atoms are removed from  $\text{LaCeO}_{3.5}$  in each pulse under a longer relaxation time, suggesting that  $\text{O}^{2-}$  diffusion is rate limiting. Lower CO selectivity after longer relaxation suggests that the non-selective pathway is more dependent on the type and concentration of oxygen species at the surface. Assuming that the injected methane pulse completely depletes the accessible surface oxygen species, the average rate of oxygen conduction to the surface is calculated to be  $2.38 \times 10^{-2}$  and  $1.52 \times 10^{-2} \mu\text{mol s}^{-1}$  during the first 30 seconds and two minutes respectively. These values are an order of magnitude lower than the initial rate of oxygen release from  $\text{LaCeO}_{3.5}$  in a redox mode ( $0.343 \mu\text{mol s}^{-1}$ ). This also explains the quick shift to a selective pathway at the initial stage of the  $\text{LaCeO}_{3.5}$  reduction in methane, *i.e.* non-selective surface oxygen species are consumed quickly due to the slow  $\text{O}^{2-}$  replenishment from the bulk.

The presence of Rh significantly enhances the performance of the redox catalyst. Not only does it increase the methane conversion, it also keeps the catalyst selective after the first pulse. Based on isotope exchange results, Rh on the surface for both redox catalysts increases the number of activated methane reaction intermediates. Such reaction intermediates are likely to be highly effective for oxygen removal from the surface. The oxygen-depleted surface in turn enhances  $\text{O}^{2-}$  conduction from the bulk as evident in Fig. 7. As a result, Rh promoted redox

catalysts enter the selective region much faster than un-promoted redox catalysts (Fig. 6).

### Effect of reaction temperature on redox properties

To further illustrate the effect of Rh, redox experiments were performed at lower temperatures (Fig. 8). Product profiles are provided in Fig. S10.† As expected, the  $\text{CaMnO}_3$  redox catalyst exhibits lower activity for methane conversion at lower temperatures. A significant drop in CO selectivity is also observed (Table 3). At lower temperatures, slower oxygen extraction may be expected to contribute to a higher POX selectivity. However,  $\text{CaMnO}_3$ , which is a known low temperature chemical looping combustion material,<sup>7,39</sup> appears to activate methane for deep oxidation until the surface and loosely bound oxygen is depleted. After that, the redox catalyst doesn't show any activity. This implies that the surface of the catalyst cannot be replenished with bulk lattice oxygen either because of the  $\text{O}^{2-}$  diffusivity at these temperatures, or smaller driving force for  $\text{O}^{2-}$  conduction.

Redox experiments on the Rh-promoted samples showed more significant effects at lower temperatures (Fig. 8). As shown in Table 3, unlike the un-promoted  $\text{CaMnO}_3$ , the CO selectivity of the promoted samples meaningfully increases with decreasing temperature. Decreasing the temperature suppresses the initial  $\text{CO}_2$  formation and elongates the selective region (Fig. S11†). While the un-promoted  $\text{CaMnO}_3$  sample did not show noticeable activity at temperatures lower than  $700^\circ\text{C}$ ,

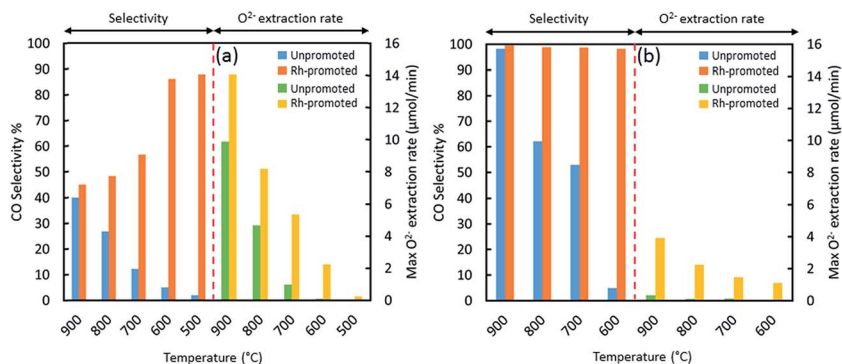


Fig. 8 Comparison of the CO selectivity and maximum oxygen donation rate of the (a)  $\text{CaMnO}_3$ -based and (b)  $\text{LaCeO}_{3.5}$ -based redox catalysts at different temperatures.

**Table 3** Methane conversion, CO/H<sub>2</sub> selectivity, oxygen donation, and coke formation of the CaMnO<sub>3</sub>-based redox catalysts during the reduction half cycle

Temperature		CO selectivity%	H <sub>2</sub> selectivity% (excluding coke)	H <sub>2</sub> selectivity% (including coke)	CH <sub>4</sub> converted (ml)	O <sub>2</sub> extracted (wt%)	Coke formation (wt%)
Un-promoted	900	40.08	29.34	37.18	2.13	9.18	0.29
	800	26.85	15.71	20.73	1.80	8.79	0.12
	700	12.28	10.94	13.24	0.80	4.14	0.02
Rh-promoted	900	44.93	40.30	46.47	2.59	10.17	0.32
	800	48.23	58.49	62.54	2.57	8.62	0.30
	700	56.63	74.70	76.64	2.86	7.93	0.25
	600	86.10	97.14	97.17	3.68	6.29	0.04
	500	87.90	100.00	100.00	1.39	2.02	0.00

**Table 4** Methane conversion, CO/H<sub>2</sub> selectivity, oxygen donation, and coke formation of the LaCeO<sub>3.5</sub>-based redox catalysts during the reduction half cycle (the selectivities of un-promoted samples at 800 and 700 °C are not very accurate due to low signal to noise ratios)

Temperature		CO selectivity%	H <sub>2</sub> selectivity% (excluding coke)	H <sub>2</sub> selectivity% (including coke)	CH <sub>4</sub> converted (ml)	O <sub>2</sub> extracted (wt%)	Coke formation (wt%)
Un-promoted	900	98.21	86.76	87.69	2.13	3.91	0.17
	800	62.10	59.16	63.66	0.32	0.99	0.02
	700	52.93	36.50	44.43	0.31	1.2	0.03
Rh-promoted	900	99.46	90.11	91.26	2.54	4.36	0.36
	800	99.60	100.00	100.00	2.10	2.60	0.21
	700	99.34	100.00	100.00	1.85	1.94	0.19

the Rh-promoted sample exhibits high methane conversion and selectivity at 600 °C. The redox catalyst remains active and selective at 500 °C (Fig. S12<sup>†</sup>). At lower than 500 °C, slow kinetics hindered the reaction and reduced methane conversion. The lower reaction temperature and less reduced surface lead to less coke formation. The above results show that at 700 °C and lower, the presence of Rh significantly increases the oxygen release of CaMnO<sub>3</sub>.

A similar trend is observed on the LaCeO<sub>3.5</sub>-based samples with more significant kinetic improvement (Fig. S13<sup>†</sup>). While the un-promoted samples show very little activity at 800 °C and below, the promoted samples remained active down to 600 °C with the initial oxygen release rate higher than that of the un-promoted sample at 900 °C (Fig. 8b and Table 4). This, again, confirms that providing methane activation sites on the surface allows for more oxygen extraction from the redox catalysts even at lower temperatures. It is concluded that activation of the C–H bond enhances oxygen removal from the oxide surface.

In order to differentiate the bulk and surface effects of rhodium on the redox performance of the catalysts, apparent activation energies of the lattice oxygen removal reaction and methane activation reaction are calculated for both continuous redox and pulse experiments. To do so, pulse experiments are conducted on CaMnO<sub>3</sub>-based redox catalysts at 700, 800, and 900 °C (Table S3<sup>†</sup>). While the removal of surface oxygen is dominant in the transient pulse experiments, the continuous redox reactions can be affected by both bulk thermodynamics and surface properties of the catalyst. Comparing the effects of Rh on activation energies in these two reaction modes enables us to infer the primary role of rhodium. By fitting the maximum oxygen donation or methane conversion rate of the redox

catalysts with the Arrhenius equation, the apparent activation energies for redox experiments are obtained. In the pulse injection experiments, the reaction rates are quantified by the total oxygen removal or methane conversion during the first pulse. These activation energies are summarized in Table 5.

Table 5 clearly indicates that Rh has a more pronounced effect on the apparent activation energies in pulse experiments. While the apparent activation energy reduces by about 33–50% in redox experiments, apparent activation energies derived from pulse experiments decrease by more than 95%. This strongly indicates that Rh addition significantly increases the activity for surface oxygen removal, by way of enhanced C–H bond activation. The increase in the overall redox activity of the metal oxides likely results from the enhanced surface oxygen removal. This indicates that the higher oxygen extraction rate is a direct result of a larger driving force for lattice oxygen removal, *i.e.* a higher oxygen chemical potential gradient between the bulk and the surface of the redox catalyst.

**Table 5** Activation energies of the CaMnO<sub>3</sub>-based catalysts in both redox and pulse injection configurations

Sample	Activation energy (kJ mol <sup>-1</sup> )			
	Redox (bulk + surface)		Pulse (surface)	
	O <sup>2-</sup>	CH <sub>4</sub>	O <sup>2-</sup>	CH <sub>4</sub>
Un-promoted	110.3	108.9	115.9	110.9
Rh-promoted	72.9	53.9	4.5	4.9

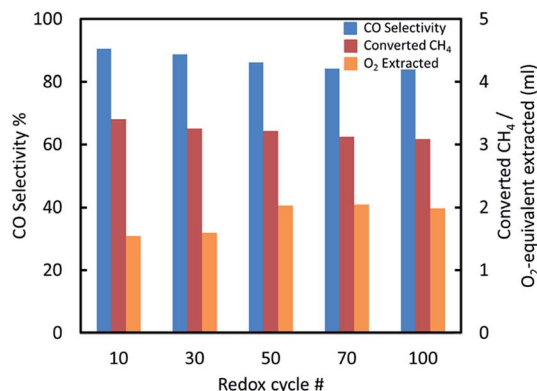


Fig. 9 Selectivity, converted methane, and O<sub>2</sub> extracted during 100 redox cycles at 600 °C on the 0.5 wt% Rh-promoted CaMnO<sub>3</sub>.

### Long term redox experiments

The aforementioned findings indicate that significantly higher syngas selectivity, lower coke formation and lower operating temperatures can be achieved by surface modification of the redox catalysts through addition of platinum group metals on their surfaces. To validate the long term performance of such redox catalysts, Rh-promoted CaMnO<sub>3</sub> is tested for extended redox cycles at 600 °C. Fig. 9 shows the selectivity and methane conversion of the catalyst through 100 complete redox cycles. The redox catalyst exhibits good redox activity throughout the 100 redox cycles. Syngas selectivity was maintained at above 94% throughout the 100 cycles. A slight decrease in syngas productivity and oxygen carrying capacity was observed, which may have resulted from sintering the redox catalyst. At the 100<sup>th</sup> cycle, the sample exhibited a syngas productivity of 7.9 mmol syngas per gram redox catalyst at 600 °C. To compare, a recently reported perovskite based redox catalyst exhibits 4.8 mmol g<sup>-1</sup> syngas productivity at 900 °C.<sup>27</sup>

## Conclusion

This article investigates the effects of rhodium on the methane POx performance of CaMnO<sub>3</sub> and LaCeO<sub>3.5</sub> redox catalysts. Significant enhancements in the redox activity and syngas selectivity are observed for both redox catalysts after addition of 0.5 wt% Rh. Experimental studies indicate that conduction of bulk lattice oxygen to the oxide surface limits the overall redox reaction rate. Meanwhile, syngas selectivity is determined by the type and abundance of surface oxygen species, which are determined by the relative rates of bulk oxygen conduction and surface oxygen removal under the dynamic redox reactions. Isotope exchange, XPS, and DRIFTS studies confirm the presence and enrichment of Rh on the surface, which is shown to significantly enhance methane C–H bond activation. This leads to higher concentrations of surface CH<sub>x</sub> species for facile oxygen extraction from the surface. The more oxygen-deprived surface in the presence of Rh imposes a higher oxygen chemical potential gradient between the oxide bulk and surface, thereby resulting in enhanced O<sup>2-</sup> conduction through the bulk of the redox catalyst. As a result, higher redox activity as well as

increased oxygen donation and selectivity were observed for Rh promoted redox catalysts at temperatures as low as 500 °C. When compared to unpromoted CaMnO<sub>3</sub> which demonstrates 2.4 mmol g<sup>-1</sup> syngas productivity at 900 °C, the Rh-promoted CaMnO<sub>3</sub> produces syngas at 7.9 mmol g<sup>-1</sup> at 600 °C with satisfactory long-term redox performance.

## Acknowledgements

This work was supported by the U.S. National Science Foundation (Award No. CBET-1254351) and Kenan Institute. The authors acknowledge the use of the Analytical Instrumentation Facility (AIF) at North Carolina State University, which is supported by the State of North Carolina and the National Science Foundation. The authors also would like to acknowledge the assistance from Dr Tianyang Li in XRD and Dr Fang He and Kun Zhao at the Guangzhou Institute of Energy Conversion, Chinese Academy of Sciences for XPS analysis.

## References

- 1 *International Energy Outlook 2016, Natural Gas - Energy Information Administration*, available at, [http://www.eia.gov/forecasts/ieo/nat\\_gas.cfm](http://www.eia.gov/forecasts/ieo/nat_gas.cfm), accessed: 5th October 2016.
- 2 M. C. Alvarez-Galvan, N. Mota, M. Ojeda, S. Rojas, R. M. Navarro and J. L. G. Fierro, *Catal. Today*, 2011, **171**, 15–23.
- 3 W.-C. Chung and M.-B. Chang, *Renewable Sustainable Energy Rev.*, 2016, **62**, 13–31.
- 4 Y. H. Hu and E. Ruckenstein, *Adv. Catal.*, 2004, **48**, 297–345.
- 5 M.-S. Fan, A. Z. Abdullah and S. Bhatia, *ChemCatChem*, 2009, **1**, 192–208.
- 6 J. Zhang and F. Li, *Appl. Catal., B*, 2015, **176–177**, 513–521.
- 7 J. Adanez, A. Abad, F. Garcia-Labiano, P. Gayan and L. F. de Diego, *Prog. Energy Combust. Sci.*, 2012, **38**, 215–282.
- 8 M. Tang, L. Xu and M. Fan, *Appl. Energy*, 2015, **151**, 143–156.
- 9 K.-S. Kang, C.-H. Kim, K.-K. Bae, W.-C. Cho, S.-H. Kim and C.-S. Park, *Int. J. Hydrogen Energy*, 2010, **35**, 12246–12254.
- 10 H.-J. Ryu and G.-T. Jin, *Korean Chem. Eng. Res.*, 2004, **42**, 588–597.
- 11 J. Adanez, L. F. de Diego, F. Garcia-Labiano, P. Gayan, A. Abad and J. M. Palacios, *Energy Fuels*, 2004, **18**, 371–377.
- 12 K. Shah, B. Moghtaderi and T. Wall, *Energy Fuels*, 2012, **26**, 2038–2045.
- 13 K. Zhang, J. Sunarso, Z. Shao, W. Zhou, C. Sun, S. Wang and S. Liu, *RSC Adv.*, 2011, **1**, 1661–1676.
- 14 P. Cho, T. Mattisson and A. Lyngfelt, *Ind. Eng. Chem. Res.*, 2005, **44**, 668–676.
- 15 P. Gayan, L. F. de Diego, F. Garcia-Labiano, J. Adanez, A. Abad and C. Dueso, *Fuel*, 2008, **87**, 2641–2650.
- 16 T. Mattisson, M. Johansson and A. Lyngfelt, *Fuel*, 2006, **85**, 736–747.
- 17 A. R. Oller, M. Costa and G. Oberdörster, *Toxicol. Appl. Pharmacol.*, 1997, **143**, 152–166.
- 18 F. Garcia-Labiano, L. F. de Diego, P. Gayan, J. Adanez, A. Abad and C. Dueso, *Ind. Eng. Chem. Res.*, 2009, **48**, 2499–2508.

- 19 H. Tian, T. Simonyi, J. Poston and R. Siriwardane, *Ind. Eng. Chem. Res.*, 2009, **48**, 8418–8430.
- 20 N. L. Galinsky, Y. Huang, A. Shafieifarhood and F. Li, *ACS Sustainable Chem. Eng.*, 2013, **1**, 364–373.
- 21 A. Shafieifarhood, N. Galinsky, Y. Huang, Y. Chen and F. Li, *ChemCatChem*, 2014, **6**, 790–799.
- 22 A. Shafieifarhood, J. C. Hamill, L. M. Neal and F. Li, *Phys. Chem. Chem. Phys.*, 2015, **17**, 31297–31307.
- 23 A. Shafieifarhood, A. Stewart and F. Li, *Fuel*, 2015, **139**, 1–10.
- 24 L. M. Neal, A. Shafieifarhood and F. Li, *ACS Catal.*, 2014, **4**, 3560–3569.
- 25 N. L. Galinsky, A. Shafieifarhood, Y. Chen, L. Neal and F. Li, *Appl. Catal., B*, 2015, **164**, 371–379.
- 26 L. Neal, A. Shafieifarhood and F. Li, *Appl. Energy*, 2015, **157**, 391–398.
- 27 A. Mishra, N. Galinsky, F. He, E. E. Santiso and F. Li, *Catal. Sci. Technol.*, 2016, **6**, 4535–4544.
- 28 N. Galinsky, A. Mishra, J. Zhang and F. Li, *Appl. Energy*, 2015, **157**, 358–367.
- 29 S. Luo, L. Zeng, D. Xu, M. Kathe, E. Chung, N. Deshpande, L. Qin, A. Majumder, T.-L. Hsieh, A. Tong, Z. Sun and L.-S. Fan, *Energy Environ. Sci.*, 2014, **7**, 4104–4117.
- 30 A. Erdohelyi, J. Cserenyi and F. Solymosi, *J. Catal.*, 1993, **141**, 287–299.
- 31 J. R. Rostrupnielsen and J. H. B. Hansen, *J. Catal.*, 1993, **144**, 38–49.
- 32 J. T. Richardson and S. A. Paripatyadar, *Appl. Catal.*, 1990, **61**, 293–309.
- 33 J. Wei and E. Iglesia, *J. Catal.*, 2004, **225**, 116–127.
- 34 G. Wang, M. Chen and M. Zhou, *Chem. Phys. Lett.*, 2005, **412**, 46–49.
- 35 Z. L. Zhang, V. A. Tsipouriari, A. M. Efstathiou and X. E. Verykios, *J. Catal.*, 1996, **158**, 51–63.
- 36 E. P. J. Mallens, J. H. B. J. Hoebink and G. B. Marin, *J. Catal.*, 1997, **167**, 43–56.
- 37 H. Y. Wang and E. Ruckenstein, *J. Catal.*, 1999, **186**, 181–187.
- 38 C. T. Au and H. Y. Wang, *J. Catal.*, 1997, **167**, 337–345.
- 39 Q. Imtiaz, D. Hosseini and C. R. Müller, *Energy Technol.*, 2013, **1**, 633–647.
- 40 S. Bhavsar, N. Isenberg, A. More and G. Veser, *Appl. Energy*, 2016, **168**, 236–247.
- 41 A. Hedayati, A.-M. Azad, M. Rydén, H. Leion and T. Mattisson, *Ind. Eng. Chem. Res.*, 2012, **51**, 12796–12806.
- 42 Z. Gu, K. Li, H. Wang, Y. Wei, D. Yan and T. Qiao, *Kinet. Catal.*, 2013, **54**, 326–333.
- 43 K.-S. Kang, C.-H. Kim, K.-K. Bae, W.-C. Cho, W.-J. Kim, Y.-H. Kim, S.-H. Kim and C.-S. Park, *Int. J. Hydrogen Energy*, 2010, **35**, 568–576.
- 44 K. Otsuka, T. Ushiyama and I. Yamanaka, *Chem. Lett.*, 1993, **22**, 1517–1520.
- 45 K. Otsuka, Y. Wang, E. Sunada and I. Yamanaka, *J. Catal.*, 1998, **175**, 152–160.
- 46 V. Bellière, G. Joorst, O. Stephan, F. M. F. de Groot and B. M. Weckhuysen, *J. Phys. Chem. B*, 2006, **110**, 9984–9990.
- 47 Y. Nishihata, J. Mizuki, T. Akao, H. Tanaka, M. Uenishi, M. Kimura, T. Okamoto and N. Hamada, *Nature*, 2002, **418**, 164–167.